Theory of lasing in a multiple-scattering medium

Sajeev John and Gendi Pang

Department of Physics, University of Toronto, Toronto, Ontario, Canada M5S 1A7

In several recent experiments, isotropic lasing action was observed in paints that contain rhodamine 640 dye molecules in methanol solution as gain media and titania particles as optical scatterers. These so-called paint-on laser systems are extraordinary because they are highly disordered systems. The microscopic mechanism for laser activity and the coherence properties of light emission in this multiple-light-scattering medium have not yet been elucidated. In this paper we derive the emission intensity properties of a model dye system with excited singlet and triplet electronic energy levels, which is immersed in a multiple-scattering medium with transport mean free path l^*. Using physically reasonable estimates for the absorption and emission cross section for the singlet and triplet manifolds, and the singlet-triplet intersystem crossing rate, we solve the nonlinear laser rate equations for the dye molecules. This leads to a diffusion equation for the light intensity in the medium with a nonlinear intensity-dependent gain coefficient. Using this model we are able to account for nearly all of the experimentally observed properties of laser paint reported so far when $l^* \gg \lambda_0$, the emission wavelength. This includes the dependence of the peak intensity of amplified emission on the mean free path l^*, the dye concentration ρ, and the pump intensity characteristics. Our model recaptures the collapse of the emission linewidth at a specific threshold pump intensity and describes how this threshold intensity varies with l^*. In addition, our model predicts a dramatic increase in the peak intensity and a further lowering of the lasing threshold for the strong scattering limit $l^* \to \lambda_0$. This suggests a striking enhancement of the characteristics of laser paint near the photon localization threshold in a disordered medium. [S1050-2947(96)07510-5]

PACS number(s): 42.55.Mv, 42.70.Hj, 78.90.+t

I. INTRODUCTION

Recently, Lawandy *et al.* reported [1] the observation of laserlike emission in a multiple-light-scattering dielectric microstructure consisting of rhodamine 640 (R640) dye molecules (in methanol) and a titanium oxide (TiO_2) colloidal suspension. This remarkable observation provides a compelling starting point for the investigation of disordered dielectric microstructures as alternative sources of coherent light emission [1,2]. Weak scattering of light has traditionally been considered detrimental to laser action since such scattering removes photons from the lasing mode of a conventional cavity. On the other hand, if stronger, multiple scattering occurs, these photons may return to the amplification region and the amplified mode itself may consist of a multiple-scattering path. Under suitable circumstances, the detrimental effects of diffuse scattering and other losses may be offset by the long path length of photons within the gain region giving rise to amplified laserlike emission. While the coherence properties of light emitted by laser paint have not yet been established, it is plausible that a continuous crossover takes place in these emission properties as the photon transport mean free path l^* is decreased. This is the crossover from amplified spontaneous emission, well known in pure dye systems with no scatterers [3], to true laserlike coherent emission as l^* approaches the emission wavelength λ_0 with a high density of scatterers. At the threshold for photon localization [4,5], the diffusion modes of light interfere strongly and are converted into a continuous spectrum of localized cavity modes in the extended medium, in which the emitted light may self-organize into a coherent state. This

scenario suggests that some striking effects may be observed if the current experiments on laser paints are repeated in more strongly scattering dielectrics.

Since the early observation of the paint-on lasers in [1,2], several subsequent experiments have been carried out [6–9]. Most of these experiments have confirmed the laserlike amplification in strongly scattering systems which contain R640 in methanol solution as gain media and titania particles as optical scatterers. Emission from this system exhibits spectral and temporal properties characteristic of a multimode laser oscillator, even though the system contains no true cavity mode. The peak emission and linewidth were observed to depend sensitively on the densities of the titania particles in the system. We list below some of the main experimental observations.

(a) There exists a well-defined threshold pump intensity above which the emission characteristics from the disordered medium change dramatically. In a wide range above the threshold, the emission at the peak wavelength (620 nm) increases much more rapidly with the pump intensity (at 532 nm) than it does below the threshold. The linewidth of the emission spectrum collapses from about 60 to 6 nm near the threshold [2,6,8,9].

(b) The emission is, in general, bichromatic and the number of emission peaks depends on dye concentration and pump intensity [8]. At a high dye concentration ($\rho = 2.5 \times 10^{-2} M$), in the disordered medium, there are two peaks. The larger peak is at 620 nm and the smaller one at 650 nm. At low dye concentrations ($\rho = 1.0 \times 10^{-3} M$ or less), there is only one peak at 620 nm.

(c) For the scattering particle densities used in the experi-

ments, the emission at the peak wavelength (620 nm) is increased with the increase of the particle density [2].

(d) The emission linewidth depends on the particle density. However, different experiments give seemingly contradictory results on whether the emission linewidth is decreased or increased with the increase of scatterer density [2,7].

The possibility of generation of amplified light by a random scattering medium with gain was suggested over 25 years ago by Letokhov [10]. He suggested that frequency stabilization could be achieved in a Doppler-broadened gain medium by means of diffusive light scattering. Nevertheless, a quantitative theory of paint-on lasers has not yet been fully elucidated. This is partly because the recently discovered paint-on laser systems cover a broad range of scattering strengths. Amplified emission has been reported both in the diffusive regime where the emission wavelength λ_0 is much smaller than the transport mean free path l^*, which in turn is smaller than the sample size L, and in the nondiffusive regime $l^* \gtrsim L$. In this paper we adopt the view that amplified emission in the nondiffusive regime is a precursor to laser activity in the fully developed diffusion regime. In this paper, we construct a nonlinear model that quantitatively recaptures the experimental results. In this model, light propagation in the paint-on laser systems is described in the diffusion approximation and we introduce a generic model for the dye, which has singlet and triplet electronic excitations and an adjustable intersystem crossing rate between these electronic states. Strictly speaking, the diffusion approximation is only valid in the case when the sample size is much larger than the transport mean free path. Nevertheless, our numerical calculations suggest that this approximation recaptures experimental results even when the sample size is only a few transport mean free paths. The properties of the dye solution enter the nonlinear diffusion equation through the gain coefficient. This gain coefficient is determined from a generic dye laser scheme [11] that produces bichromatic emission from the singlet states and the triplet states. We assume that there is a steady-state dye population in the triplet states that also participate in the stimulated-emission process. Although this is not the only possible model leading to the observed bichromatic emission, we believe that it is the most natural. Another possibility is that the second peak at 650 nm arises from a transition from a higher excited state within the singlet manifold. However, Sha, Liu, and Alfano have observed [8] that, in the neat dye at high dye concentration and high pump intensities, lasing occurs first at 650 nm. This is suggestive of a metastable triplet state population that exceeds the population of the singlet excited state. Our model leads to a set of coupled diffusion equations for photons with different frequencies. They constitute a highly nonlinear set of differential equations. Numerical solution of these equations yields good agreement with the experiments. Our theory also gives several predictions that may be tested by future experiments. In particular we have extrapolated the diffusion model into the regime ($l^* \to \lambda_0$) of incipient photon localization [4]. We find that the singlet peak emission increases with (λ_0/l^*) as a power law. This suggests the possibility of further synergy between photon localization and laser activity if wave interference corrections to diffusion are included. The interplay between photon localization and photon ab-
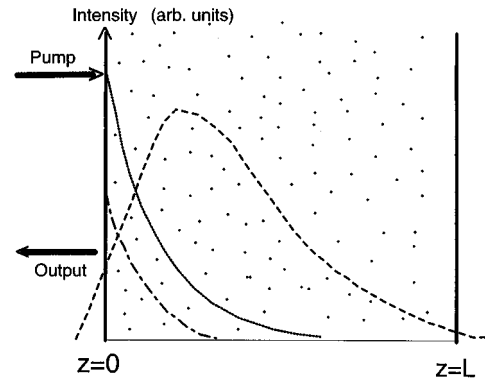

FIG. 1. Schematic view of the sample showing the pump intensity $P(z)$ (solid line), the spontaneous-emission source intensity $\int d\hat{q}\, S_w(z,\hat{q})$ (dot-dashed line), and the stimulated emission intensity profile $I(\omega,z)$ (dashed line). The magnitudes of the respective curves are in arbitrary units and are not to scale.

sorption in a passive medium (white paint) has been discussed by Anderson [12] and John [13].

II. MODEL

In our model we assume that the absorbing dye solution with scattering titania particles fills the entire sample region between the two planes $z=0$ and L (see Fig. 1). We define $z<0$ as the left region and $z>0$ as the right region. A monochromatic pumping beam with frequency ν_0 is incident from the left and is collimated in the direction perpendicular to the $z=0$ plane. The light intensity emitted from the front (or left) plane is measured by a detector on the left [14]. This geometry is close to that of the cells used in recent experiments. We assume that the whole system is homogeneous in the x and y directions. Since the wavelength (532 nm) of the pumping laser beam is outside the emission spectrum of the R640 dye solution, there is no coherence between the pumping beam and the emission rays in the experimental system. We note, by way of contrast, that some recent experiments [15,16] have used an additional probe beam to investigate the coherent backscattering of light from amplifying random media. We plan to discuss this coherent-backscattering problem in a future paper.

The physical picture of the system is as follows. The dye molecules absorb energy from the pumping beam and are excited to higher states. Then, through spontaneous emission, some excited molecules randomly emit photons with frequencies different from that of the pumping beam. These photons travel in the medium, being scattered by the titania particles and amplified by the dye solution through the stimulated-emission process, and finally leave the medium and reach the detector. Accordingly, the emergent photon energy (from the medium) per unit time, unit solid angle, and unit interface area around the direction $\hat{k}_f$ in the frequency range from ω to $\omega+d\omega$ can be expressed as

$$I_{\text{output}}(\omega,\hat{\vec{k}}_f)d\omega = \frac{c}{4\pi l^*} \int dz \int d^3\vec{r}' \int d\hat{\vec{q}}[S_\omega(\vec{r}',\hat{\vec{q}})d\omega]$$

$$\times G_\omega(\vec{r}-\vec{r}';\hat{\vec{q}},\hat{\vec{k}}_f)\exp\left(-\frac{z}{|\hat{\vec{k}}_f\cdot\hat{\vec{z}}|l^*}\right).$$

$$(1)$$

Here $z = \vec{r}\cdot\hat{\vec{z}}$ with $\hat{\vec{z}}$ being the unit vector of the z axis, c is the velocity of light, l^* is the transport mean free path [17], and $S_\omega(\vec{r}',\hat{\vec{q}})d\omega$ is the source intensity within the sample (energy per unit volume, per unit time, and per unit solid angle around the direction $\hat{\vec{q}}$, in the frequency range from ω to $\omega+d\omega$) due to spontaneous emission. This source intensity is proportional to the density of excited dye molecules at position $\vec{r}'$ and their spontaneous-radiative-emission cross section at frequency ω and direction $\hat{\vec{q}}$. It does not include stimulated emission since all stimulated processes will be accounted for in the propagator $G_\omega(\vec{r}-\vec{r}';\vec{q},\hat{\vec{k}}_f)$. The factor $\exp(-z/|\hat{\vec{k}}_f\cdot\hat{\vec{z}}|l^*)$ represents the part of the photon flux that emerges coherently without being further scattered [17]. The Green's function $G_\omega(\vec{r}-\vec{r}';\hat{\vec{q}},\hat{\vec{k}}_f)$ in (1) describes the propagation of the photons through the gain region from position $\vec{r}'$ with wave vector $(\omega/c)\hat{\vec{q}}$ to position $\vec{r}$ with wave vector $(\omega/c)\hat{\vec{k}}_f$. In the diffusion approximation [18], G_ω is independent of the wave vectors, i.e., $G_\omega(\vec{r}-\vec{r}';\hat{\vec{q}},\hat{\vec{k}}_f) = G_\omega(\vec{r}-\vec{r}')$, and satisfies the diffusion equation

$$D\vec{\nabla}_r^2 G_\omega(\vec{r}-\vec{r}') + \frac{c}{l_g(\omega,z)} G_\omega(\vec{r}-\vec{r}') = -\delta(\vec{r}-\vec{r}'), \quad (2)$$

with boundary conditions

$$G_\omega(\vec{r}-\vec{r}')_{\vec{r}\cdot\hat{\vec{z}}=-0.71l^*} = G_\omega(\vec{r}-\vec{r}')_{\vec{r}\cdot\hat{\vec{z}}=L+0.71l^*} = 0. \quad (3)$$

Here $D=\frac{1}{3}cl^*$ is the classical diffusion constant, which we assume is not altered by the presence of the dye. This approximation is valid for low dye concentrations and low pump intensities. $l_g^{-1}(\omega,z)$, which has the dimension of inverse length, is the gain coefficient of the dye solution. l_g may depend on the coordinate z as well as the local light intensity and will be determined in the following paragraphs. In (3), we have introduced two ''trapping planes,'' located at $d_1=-0.71l^*$ and $d_2=L+0.71l^*$, respectively, at which the Green's function has zero value. This imposes the physical boundary condition that photons that come within a mean free path of the same boundary leave the sample and are effectively ''absorbed'' by the external vacuum. This factor of $0.71l^*$ arises because the photon density cannot vanish exactly at the sample surface. Photons diffuse out of the medium and must pass through the surface. The values of d_1 and d_2 may be obtained from the method of linear extrapolation and a detailed derivation of the ''trapping plane'' positions can be found in [19]. We note here that a more rigorous treatment of the boundary-layer problem can be found in [20]. We also note that the diffusion equation (2) can be derived from the more general radiative transfer theory in the
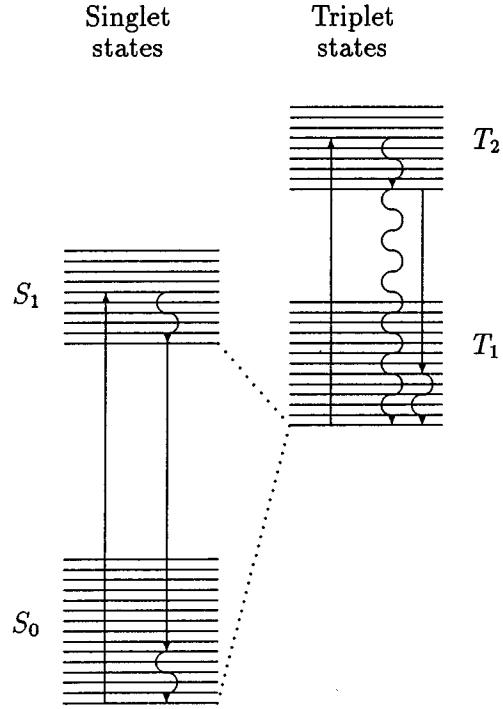

FIG. 2. Typical energy levels for a dye in solution and the proposed laser scheme for laser paint. The singlet and triplet levels are shown in separate columns. $S_0\rightarrow S_1$ represents the pumping process, $S_1\rightarrow S_0$ and $T_2\rightarrow T_1$ represent the emission process, and $T_1\rightarrow T_2$ represents the absorption process. The wiggly arrows represent the nonradiative decay processes. The dotted lines represent the intersystem crossing process.

P_1 approximation [21]. This in turn is an approximation to the more general coherence propagation theory for the electric-field autocorrelation function. The approximation becomes valid in the limit when the physical length scale of interest is much longer than the transport mean free path [22,23]. The more rigorous coherence theory involving the electric field rather than the intensity of light is necessary to fully elucidate the coherence properties of the amplified light as well as to fully describe the *weak* multiple-scattering regime $l^*\gtrsim L$. It leads to a distinction between the *scattering* mean free path l and the *transport* mean free path l^* that is apparent whenever the scattering particles have nontrivial structure and nontrivial spatial correlations. It also leads to corrections to the classical diffusion coefficient arising from the presence of the dye. However, for simplicity we consider only a ''white-noise'' model for the disorder in which $l^*=l$. This diffusion model accurately recaptures most of the experimental features discussed in the literature so far.

The typical energy levels [11] for a dye in solution is shown in Fig. 2, where we keep only the energy bands that are relevant to the lasing mechanism. The horizontal lines in the figure represent vibrational sublevels of the electronic states. The very closely spaced rotational sublevels between two vibrational sublevels are not shown in the figure. The singlet and triplet states refer to the fact that the total electronic spin of the dye molecule in these states is 0 and 1, respectively (the total spin of the dye molecule in the ground state is zero and only one electron can be excited).

The lasing scheme we use to model R640 dye solution (see Fig. 2) has been successfully applied to a variety of other dyes [11]. The inclusion of a triplet excited-state manifold is motivated entirely by the observation of bichromatic emission in R640. It is experimentally observed [8] that, at a high dye concentration, both the 620- and 650-nm peaks rapidly increase with the pumping intensity. More importantly, the ratio between the heights of these two peaks remains nearly constant when the pumping intensity is greater than a threshold value. This is suggestive of a separate emission process. If there is only one emission process involved, then any modification of the cross sections will not give increasing peaks with constant peak height ratio. Therefore, we assume that in addition to the nonradiative decay to T_1 states, molecules in the T_2 states can also participate in the (spontaneous and stimulated) emission process giving rise to the secondary laser emission peak at 650 nm. Of course, the inclusion of the triplet manifold is not the only possible model yielding two separate lasing peaks. An alternative is to consider the possible emission process in the higher-energy band S_2 of the singlet manifold. However, we believe that this possibility is less likely to account for the fact under certain circumstances [8], the 650-nm laser emission occurs *prior* to the 620-nm laser emission. The triplet state $T_2 \rightarrow T_1$ emission involves levels that have lower energy than those of the $S_2 \rightarrow S_1$ emission and accordingly is thermodynamically more likely. This is also evident in detailed studies of rhodamine 6G [24], where it was necessary to depopulate the triplet state by collisional deexcitation using chemical additives before a significant population in the S_2 level could be achieved. It would be useful in the present context to add similar triplet state quenchers to isolate the possible contributions from $S_2 \rightarrow S_1$ and $T_2 \rightarrow T_1$ to the 650-nm lasing peak. Another alternative is to consider the possible existence of excimers that may be created by chemical reactions between certain excited dye molecules and those in the ground-states [25]. These excimers, once created, may dissociate into ground-state monomers by emitting an extra photon, which can form a new emission band. However, the existence of this type of emission process in the present paint-on laser systems is purely speculative and we will not discuss it here. We will show below the inclusion of the triplet manifold with an adjustable singlet-triplet intersystem crossing rate is sufficient to explain the 650-nm peak observed in the experiments.

It will be seen in the following that the emission from the triplet states plays a very important role in the lasing behavior of the system even when the nonradiative decay rate from the T_2 to the T_1 states is very large. We assume that the intersystem crossing process from T to S (or S to T) due to collisions among molecules is very slow (typically around 10^{-8}–10^{-7} s for $S_1 \rightarrow T_1$ and 10^{-7}–10^{-3} s for $T_1 \rightarrow S_0$), when compared to the radiative emission processes within T and S (typically around 10^{-9} s). This slow intersystem crossing is the generic behavior of many other well-studied dyes. For example, the inverse of the intersystem crossing rate from S_1 to T_1 for rhodamine 6G is 6.25×10^{-8} s [11]. Consequently, there is a nontrivial, adiabatically varying, triplet population throughout the pulse duration of the pumping beam used in the experiments [1,2,6–9]. We consider the case in which the pulse duration of the pumping beam is shorter than the inverse of the intersystem crossing rate. This is clearly manifest for the picosecond to nanosecond pulses used in paint-on lasers [1,2,6–9]. In this case, it can be shown that there are effectively $\eta N_2^{(S)}$ dye molecules remaining in the triplet states during the pulse, where $N_2^{(S)}$ is the population at the lowest sublevel in S_1 (the population remaining in the singlet states is therefore $N - \eta N_2^{(S)}$, where N is the total population of the dye molecules). The nature of the adiabatically varying triplet population is demonstrated using a simple model in the Appendix. Here η may depend on the pulse duration and the dye concentration and we consider it as an adjustable parameter in this paper. In the $S_2 \rightarrow S_1$ lasing transition scenario, $\eta N_2^{(S)}$ would represent the number of molecules excited into the S_2 manifold rather than into the T_1 manifold.

For the time scales given by Eq. (A1) in the Appendix, we can write the laser rate equations for the singlet and triplet states separately by assuming that the total populations in the singlet and triplet states are $\eta N_2^{(S)}$ and $N - \eta N_2^{(S)}$, respectively. For the nanosecond duration pump beam pulse used in most experiments, Eq. (A1) is a realistic approximation. The laser rate equations for the singlet states can be written as (omitting the dependence on spatial coordinate z)

$$\frac{d}{dt} N_0^{(S)} = -PN_0^{(S)} + \sum_\omega \Gamma_{10}^{(S)}(\omega) N_1^{(S)}(\omega),$$

$$\frac{d}{dt} N_2^{(S)} = PN_0^{(S)} - \Gamma_2^{(S)} N_2^{(S)}$$

$$- \sum_\omega \sigma_e^{(S)}(\omega)[N_2^{(S)} - N_1^{(S)}(\omega)]\Phi(\omega), \quad (4)$$

$$\frac{d}{dt} N_1^{(S)}(\omega) = -\Gamma_{10}^{(S)}(\omega) N_1^{(S)}(\omega) + \Gamma_{21}^{(S)}(\omega) N_2^{(S)} + \sigma_e^{(S)}(\omega)$$

$$\times [N_2^{(S)} - N_1^{(S)}(\omega)]\Phi(\omega).$$

Here $N_0^{(S)}$ is the population in the ground state, $N_2^{(S)}$ the population in the lowest level in the S_1 manifold, and $N_1^{(S)}(\omega)$ denotes the population in a particular state of the S_0 manifold that is above the ground state and has the energy $\hbar\omega$ lower than the lowest level of the S_1 manifold. In (4), P is the pumping rate, $\Gamma_2^{(S)} = \Sigma_\omega \Gamma_{21}^{(S)}(\omega)$ is the total decay rate of the lowest level in the S_1 manifold due to spontaneous emission into individual levels of S_0 with individual rates $\Gamma_{21}^{(S)}(\omega)$, $\Gamma_{10}^{(S)}(\omega)$ is the nonradiative decay rate of the vibrational excited state in S_0, $\sigma_e^{(S)}(\omega)$ is the cross section (which has the dimensions of area) for stimulated emission from the bottom of the S_1 manifold to a vibration level in S_0, and $\Phi(\omega)$ is the photon flux (number of photons per unit area, per unit time) at frequency ω. The flux is related to the light intensity I through the relation $I = \hbar\omega\Phi(\omega)$. Here we have assumed that the nonradiative decay rate within S_1 is very fast (typically 10^{-13} s) and the population at the higher levels of S_1 is almost zero. In (4), we have not explicitly included the intersystem crossing rate because it is relatively small, as discussed above. We have also ignored the direct contribution from the absorption and stimulated emission between the lowest level of S_1 and the ground state. This direct process has negligible weight when compared to the indirect processes described by $\sigma_e^{(S)}(\omega)[N_2^{(S)} - N_1^{(S)}(\omega)]\Phi(\omega)$, fol-

lowed by nonradiative coupling from a vibrational state in S_0 to the ground state. Moreover, the explicit inclusion of the spontaneous emission directly from the lowest level of S_1 to the ground state in the rate equations does not change our result (5).

Replacing the index S and the quantity $PN_0^{(S)}$ in (4) by T and $\Sigma_\omega \sigma_a^T(\omega) N_0^{(T)} \Phi(\omega)$, respectively [where $\sigma_a^T(\omega)$ is the cross section for absorption within the triplet state manifold], we obtain the corresponding rate equations for the triplet states. We note here that for the triplet states, $\Gamma_2^{(T)}$ explicitly contains the nonradiative decay contribution, namely,

$$\Gamma_2^{(T)} = \gamma_2^{(T)} + \sum_\omega \Gamma_{21}^{(T)}(\omega),$$

where $\gamma_2^{(T)}$ is the rate for the nonradiative decay from the T_2 manifold to the lowest level in the T_1 manifold (see Fig. 2). We have not explicitly included the nonradiative decay from S_1 to S_0 since this is assumed to be small compared to nonradiative decay to the lowest level in S_1 followed by radiative emission to S_0 [11]. The incorporation of a nonradiative decay rate $\gamma_2^{(S)}$ from S_1 directly to S_0 leads to overall damping out of the entire gain process. This becomes most evident when $\gamma_2^{(S)} \gtrsim \Gamma_2^{(S)}$. In particular, when $\gamma_2^{(S)} \gg \Gamma_2^{(S)}$, the threshold pump intensity for laser activity is increased by a factor of $\gamma_2^{(S)}/\Gamma_2^{(S)}$, as we will discuss later. The overall physical picture is that of a four-level laser scheme consisting of the lowest levels in the S_0, S_1, T_1, and T_2 manifolds. The vibrational substructure simply provides an effective broadening of these essential states, which we include to make a quantitative comparison to experimentally observed line shapes.

Noting that the total population in the triplet states is $\eta N_2^{(S)}$ and the total population in the singlet states is $N - \eta N_2^{(S)}$, we can easily obtain the steady-state solution of the rate equations. The gain coefficient of the dye solution is defined by

$$\frac{1}{l_g(\omega,z)} \equiv \sigma_e^{(S)}(\omega)[N_2^{(S)} - N_1^{(S)}(\omega)]/V$$
$$+ \sigma_e^{(T)}(\omega)[N_2^{(T)} - N_1^{(T)}(\omega)]/V - \sigma_a^{(T)}(\omega)N_0^{(T)}/V.$$

It is straightforward to verify that

$$\frac{1}{l_g(\omega,z)} = \left[\sigma_e^{(S)}(\omega) - \eta \sigma_a^{(T)}(\omega) \right.$$
$$+ \eta \frac{[\sigma_e^{(T)}(\omega) + \sigma_a^{(T)}(\omega)]R_a^{(T)}(z)}{\Gamma_2^{(T)} + R_a^{(T)}(z) + R_e^{(T)}(z)} \right]$$
$$\times \frac{\rho P}{(1+\eta)P + \Gamma_2^{(S)} + R_a^{(S)}(z)}. \quad (5)$$

where V is the volume of the system, ρ is the dye concentration, and

$$R_\beta^{(\alpha)}(z) \equiv \sum_{\omega'} \sigma_\beta^{(\alpha)}(\omega') \Phi(\omega'), \quad \alpha = S,T; \ \beta = e,a, \quad (6)$$

is an absorption ($\beta=a$) or stimulated-emission ($\beta=e$) rate within the α-state manifold. Here we have used the fact that

the intramanifold nonradiative relaxation rates $\Gamma_{10}^{(\alpha)}$, $\alpha=S,T$, are very large (typically 10^{13} s^{-1}) and the populations in the vibrationally excited sublevels of S_0 and T_1 can be ignored. The source intensity due to spontaneous emission can likewise be expressed as

$$\int d\hat{\vec{q}} \, S_w(\vec{r},\hat{\vec{q}}) \equiv \hbar \omega [\Gamma_{21}^{(S)}(\omega)N_2^{(S)} + \Gamma_{21}^{(T)}(\omega)N_2^{(T)}]/V$$

$$= \hbar \omega \left[\Gamma_{21}^{(S)}(\omega) + \eta \frac{\Gamma_{21}^{(T)}(\omega)R_a^{(T)}(z)}{\Gamma_2^{(T)} + R_a^{(T)}(z) + R_e^{(T)}(z)} \right]$$

$$\times \frac{\rho P}{(1+\eta)P + \Gamma_2^{(S)} + R_a^{(S)}(z)}. \quad (7)$$

For real systems, the sum in (6) should be replaced by an integral and each cross section (for emission or absorption) can be expressed in the generic form [11]

$$\sigma(\omega) = \frac{2\pi^2}{3\epsilon_0 c\hbar} \int d\nu \, \mathscr{D}(\nu)|\mu|^2 g(\omega - \nu)\nu. \quad (8)$$

Here $\mathscr{D}(\nu)$ is the rovibrational density of states of the relevant energy band, μ is the transition matrix element of the electric dipole moment, ϵ_0 is the vacuum permittivity, and $g(\omega-\nu)$ is the homogeneously broadened line-shape function for a particular molecular rovibrational transition [11]. Explicit forms of these functions are discussed in Sec. III. The pumping rate in (5) is in fact a strong function of z because the pumping beam decays in the $\hat{\vec{q}}$ direction due to both the absorption by the dye molecules and scattering by the titania particles. It is given by

$$P(z) = \sigma_a(\nu_0)(\hbar \nu_0)^{-1} I_{\text{inc}} e^{-z/l_z}. \quad (9)$$

where the diffusion controlled extinction length

$$l_z \equiv (l^* l_a/3)^{1/2}.$$

Here $l_a = [(N_0^{(S)}/V)/\sigma_a(\nu_0)]^{-1} \simeq [\rho\sigma_a(\nu_0)]^{-1}$ is the absorption length and $\sigma_a(\nu_0)$ is the cross section of the singlet absorption at the pump frequency ν_0. The parameter I_{inc} in (9) is the intensity of the pumping beam at $z=0$. In this approximation, saturation, effects due to depletion of the ground-state population are not considered since we have set $N_0^{(S)}$ in the expression of l_a equal to the *total* dye concentration ρ. Saturation effects may be obtained by requiring that l_z is self-consistently determined through the laser rate equations themselves. This leads to bleaching of the dye and the pump beam can then penetrate deeper into the sample at high pump intensity. We consider, however, only the low pump intensity, short pulse duration regime relevant to the current set of experiments.

It is convenient to define the dimensionless length

$$\tilde{z} \equiv z/l_z$$

and the dimensionless intensity

$$\tilde{I}(\omega,\tilde{z}) \equiv \frac{c\sigma_{\text{max}}^{(S)}}{\hbar\omega\Gamma_2^{(S)}} \int d^3\vec{r}' \int d\hat{\vec{q}} \, S_\omega(\vec{r}',\hat{\vec{q}}) G_\omega(\vec{r}-\vec{r}';\hat{\vec{q}},\hat{\vec{k}}_f),$$

where $\sigma_{\max}^{(S)} \equiv \max[\sigma_e^{(S)}(\omega)]$. We also introduce the homogeneously broadened output intensity

$$I_{\text{out}}(\omega) \equiv \int d\hat{\vec{k}}_f \int d\overline{\omega}\, I_{\text{output}}(\overline{\omega}, \hat{\vec{k}}_f) g(\overline{\omega} - \omega). \quad (10)$$

where I_{output} is defined in (1). Using these definitions, we get the final expression for the total emergent photon energy from the front surface of the medium (per unit surface area, per unit time, in the frequency range from ω to $\omega + d\omega$)

$$I_{\text{out}}(\omega) d\omega = \frac{\hbar l_z \Gamma_2^{(S)}}{4\pi l^* \sigma_{\max}^{(S)}} d\omega \int d\hat{\vec{k}}_f \int d\overline{\omega} \int_0^{L/l_z} d\widetilde{z}\, \exp$$

$$\left(-\frac{\widetilde{z} l_z}{|\hat{\vec{k}}_f \cdot \hat{\vec{z}}| l^*} \right) \widetilde{I}(\overline{\omega}, \widetilde{z}) \overline{\omega} g(\overline{\omega} - \omega). \quad (11)$$

Here the dimensionless intensity $\widetilde{I}(\overline{\omega}, \widetilde{z})$ is the photon flux in the medium times $\sigma_{\max}^{(S)}/\Gamma_2^{(S)}$. It satisfies the dimensionless, nonlinear differential equation

$$\partial_{\widetilde{z}}^2 \widetilde{I}(\omega, \widetilde{z}) + \pi^2 \widetilde{I}_p e^{-\widetilde{z}} \frac{\beta(\omega, \widetilde{z}) \widetilde{I}(\omega, \widetilde{z}) + \gamma(\omega, \widetilde{z})}{1 + \Sigma_a(\nu_0) \widetilde{I}_p e^{-\widetilde{z}} + \widetilde{R}_e^{(S)}(\widetilde{z})} = 0, \quad (12)$$

with boundary conditions

$$\widetilde{I}(\omega, \widetilde{z})|_{\widetilde{z} = -0.71 l^*/l_z} = \widetilde{I}(\omega, \widetilde{z})|_{\widetilde{z} = (L + 0.71 l^*)/l_z} = 0. \quad (13)$$

Here

$$\widetilde{R}_\beta^{(\alpha)}(\widetilde{z}) \equiv \int d\overline{\omega}\, \frac{\sigma_\beta^{(\alpha)}(\overline{\omega})}{\sigma_{\max}^{(S)}} \widetilde{I}(\overline{\omega}, \widetilde{z}), \quad \alpha = S, T; \ \beta = a, e. \quad (14)$$

Equation (12) is obtained from the definition of $\widetilde{I}$ and the diffusion equation (2). If we measure the emission from the side windows [7], the related equation are almost the same as here except that $e^{-\widetilde{z}}$ in (12) should be dropped and L should be replaced by the actual length of the sample in the side direction.

The term that is proportional to $\beta(\omega, \widetilde{z})$ in (12) comes from the gain coefficient and the term proportional to $\gamma(\omega, \widetilde{z})$ comes from the source intensity due to the spontaneous emission. Explicitly, $\beta(\omega, \widetilde{z})$ and $\gamma(\omega, \widetilde{z})$ are given by

$$\beta(\omega, \widetilde{z}) \equiv \frac{1 + \Sigma_a(\nu_0) \widetilde{I}_p e^{-\widetilde{z}} + \widetilde{R}_e^{(S)}(\widetilde{z})}{\pi^2 \widetilde{I}_p e^{-\widetilde{z}}} \frac{l_a}{l_g(\omega, \widetilde{z})}$$

$$= (\sigma_{\max}^{(S)})^{-1} \{\sigma_e^{(S)}(\omega) - \eta \sigma_a^{(T)}(\omega) + \eta[\sigma_e^{(T)}(\omega) + \sigma_a^{(T)}$$

$$\times (\omega)] f(\widetilde{z})\} \quad (15)$$

and

$$\gamma(\omega, \widetilde{z}) \equiv \frac{1 + \Sigma_a(\nu_0) \widetilde{I}_p e^{-\widetilde{z}} + \widetilde{R}_e^{(S)}(\widetilde{z})}{\pi^2 \widetilde{I}_p e^{-\widetilde{z}}} \frac{\int d\hat{\vec{q}}\, S_\omega(\vec{r}, \hat{q})}{\hbar \omega \Gamma_2^{(S)}/l_a \sigma_{\max}^{(S)}}$$

$$= (\Gamma_2^{(S)})^{-1} [\Gamma_{21}^{(S)}(\omega) + \eta \Gamma_{21}^{(T)}(\omega) f(\widetilde{z})]. \quad (16)$$

Here

$$f(\widetilde{z}) \equiv \frac{\widetilde{R}_a^{(T)}(\widetilde{z})}{\Gamma_2^{(T)}/\Gamma_2^{(S)} + \widetilde{R}_a^{(T)}(\widetilde{z}) + \widetilde{R}_e^{(T)}(\widetilde{z})}$$

describes the fraction of the total population of the triplet manifold that is in the T_2 states. The $\Gamma_{21}^{(\alpha)}(\omega)$, $\alpha = S, T$, in the above expressions are related to $\sigma_e^{(\alpha)}(\omega)$ through the relation between the Einstein A and Einstein B coefficients [11]. The other new quantities appearing in (12) are the dimensionless incident intensity at $z = 0$

$$\widetilde{I}_p \equiv I_{\text{inc}}/\widetilde{I}_c,$$

the characteristic intensity parameter

$$\widetilde{I}_c \equiv \hbar \nu_0 \pi^2 \Gamma_2^{(S)}/\sigma_{\max}^{(S)} = \hbar \nu_0 c^{-2} \int d\omega\, \omega^2 \sigma_e^{(S)}(\omega)/\sigma_{\max}^{(S)},$$

and the dimensionless absorption cross section

$$\Sigma_a(\nu_0) \equiv (1 + \eta) \pi^2 \sigma_a^{(S)}(\nu_0)/\sigma_{\max}^{(S)}.$$

As mentioned before, we have not included in (12) the nonradiative decay from the S_1 manifold to the S_0 manifold because its rate is comparatively small in the present case. If this nonradiative decay were included, then the factor of 1 in the denominator of (12) would be replaced by $1 + \gamma_2^{(S)}/\Gamma_2^{(S)}$. When $\gamma_2^{(S)}/\Gamma_2^{(S)} \ll 1$, this additional term has little effect. When $\gamma_2^{(S)}/\Gamma_2^{(S)} \gg 1$, the effect of this additional term can be seen by simply multiplying both the denominator and the numerator in (12) by a factor $(1 + \gamma_2^{(S)}/\Gamma_2^{(S)})^{-1}$. This reveals that the effective pumping intensity will be reduced by a factor $\gamma_2^{(S)}/\Gamma_2^{(S)}$ when $\gamma_2^{(S)}/\Gamma_2^{(S)} \gg 1$.

From (12) we see that $\widetilde{I}$ is equal to zero when the pumping intensity $\widetilde{I}_p = 0$ as required. When $0 < \widetilde{I}_p \ll 1$, $\widetilde{I}$ is very small and (12) can be approximated by a linear differential equation. However, when $\widetilde{I}_p$ is close to or larger than 1, we must consider nonlinear effects and solve (12) directly. In the following we give the numerical results for the light-output intensity $I_{\text{out}}(\omega)$, which are obtained by solving (12). Equation (12) can be solved as follows: we first approximate the integral in (14) by a sum over a set of discrete frequencies ω_i, $i = 1, 2, \ldots, N$. This reduces (12) to a set of N coupled nonlinear differential equations. These coupled nonlinear differential equations can then be solved by using the shooting and matching techniques described in [26].

III. COMPARISON WITH EXPERIMENTS

Since there is not yet enough experimental data available to independently fix all of the microscopic parameters (such as the cross sections and the nonradiative decay rates) for the R640 dye solution, we make some plausible estimates. We choose the values of these parameters in order to fit a broad range of experimental data. Of course, we cannot exclude the possibility that other choices can also fit specific pieces of experimental data. In all of the following calculations, we choose $\Gamma_2^{(T)}/\Gamma_2^{(S)} = 10$, $\sigma_a^{(S)}(\nu_0)/\sigma_{\max}^{(S)} = 2$, and the line-shape function
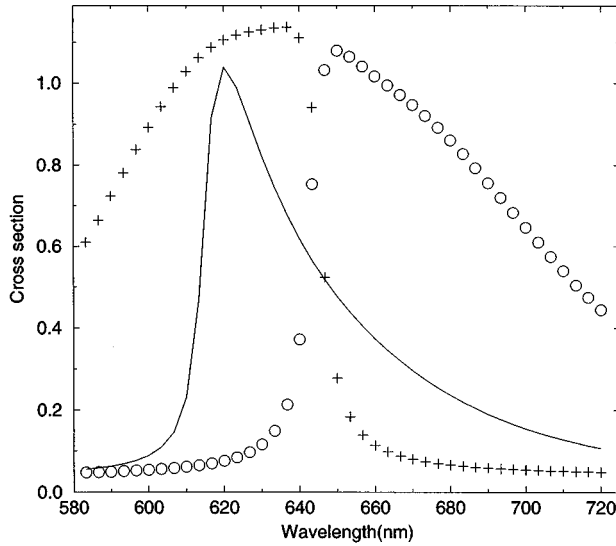
FIG. 3. Cross section of the stimulated emission from singlet states (solid line), the stimulated emission for triplet states (circles), and the triplet absorption (crosses). All the cross sections are in units of $\max(\sigma_e^{(S)})$.

$$g(\overline{\omega}-\omega)=\frac{1}{\pi}\frac{\Delta\omega}{\omega^2+(\Delta\omega)^2}, \qquad (17)$$

with $\Delta\omega=(2\pi c/\lambda_0)(6nm/2\lambda_0)$, where $\lambda_0=620$ nm. The 6-nm linewidth is chosen since it is the minimum width to which the emission narrows under strong laserlike amplification. The cross sections we used in the calculations are shown in Fig. 3. These cross sections are obtained from (8) by assuming that

$$\mathscr{D}(\nu)|\mu|^2 \propto e^{-|a(1-\nu/\omega_0)|}[1+b(1-\nu/\omega_0)^2] \qquad (18)$$

within the energy band, where a, b, and ω_0 are three adjustable parameters. Equation (18) is based on the fact that $\mathscr{D}(\nu)$ is the density of vibrational states. The excited states of an isotropic harmonic oscillator are highly degenerate and we describe this degeneracy by the quantity in square brackets in (18). This is a generic form for a three-dimensional oscillator. μ is a dipole matrix element connecting the ground and excited electronic states in different vibrational states. Accordingly, it contains a Frank-Condon [11] overlap factor $e^{-|a(1-\nu/\omega_0)|}$. The values of a, b, and $2\pi c/\omega$ are chosen as 35, 264.5, and 615 nm for $\sigma_e^{(S)}$; 35, 954.5, and 645 nm for $\sigma_e^{(T)}$; and -35, 1111, and 645 nm for $\sigma_a^{(T)}$, respectively. We choose these values in order to fit the experimental data on the positions of the emission peaks and the linewidths of the emission spectra. As in most of the experiments, we set $L=1$ cm in the calculations.

Figures 4(a) and 4(b) show how the number of emission peaks depends on the dye concentration and the parameter η. In each figure we plot the emission spectrum at nine different values of pump intensity, and the outermost curve corresponds to the pump intensity at 0.63×10^7 J cm^{-2} s^{-1} and the innermost at 0.07×10^7 J cm^{-2} s^{-1}. There are two peaks for a dye concentration of 2.5×10^{-2} M in Fig. 4(a) (the large one at 620 nm and the small one around 650 nm), while there is only one peak at 620 nm for a dye concentration of
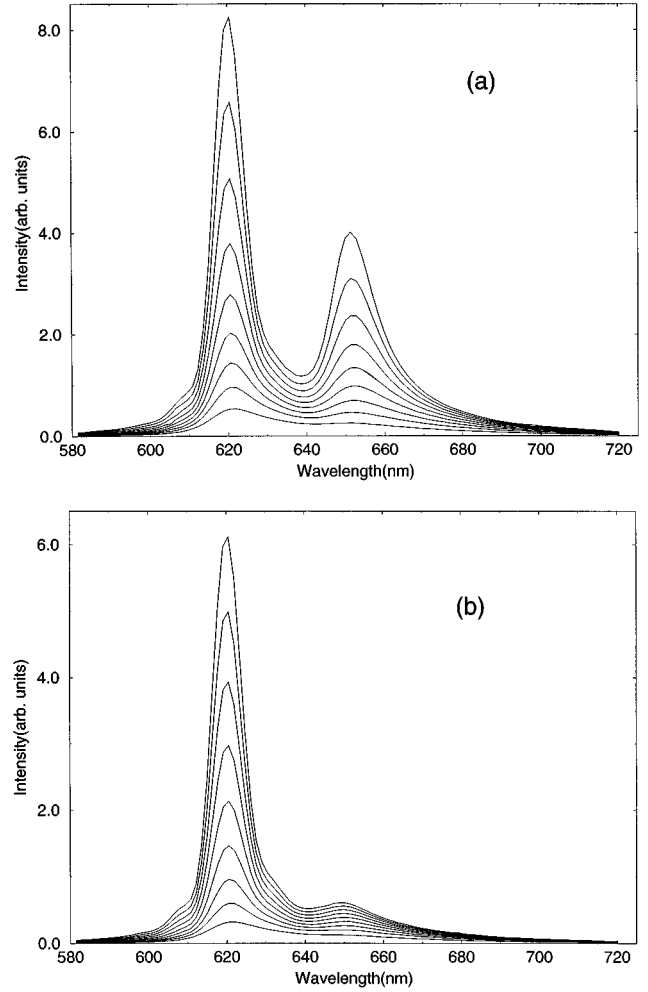

FIG. 4. Emission spectra at nine different pump intensities for two different dye concentrations: (a) high dye concentration with the absorption length $l_a=5.0\times10^{-4}$ cm and the triplet-population parameter $\eta=0.63$ and (b) low dye concentration with $l_a=2.5\times10^{-2}$ cm and $\eta=0.5$. We set the transport mean free path $l^*=1.95\times10^{-3}$ cm in the calculations. The pump intensities vary from 0.07×10^7 J cm^{-2} s^{-1} for the innermost curve to 0.63×10^7 J cm^{-2} s^{-1} for the outmost curve in each figure.

$5\times10^{-4}M$ in Fig. 4(b). The value of dye concentration for a given absorption length is estimated from the formula $l_a=[\rho\sigma_a(\nu_0)]^{-1}$ and the fact that the pump beam penetration depth of a $2.5\times10^{-3}M$ dye solution is about 50 μm [2]. These curves agree quantitatively with the experiments [8]. We note that the adjustable parameter η depends on the dye concentration in our calculation. We do not consider a microscopic model for intersystem crossing but simply treat it phenomenologically. It is plausible that intersystem crossing is driven by the rate of molecular interactions and collisions, which may in turn be enhanced when the concentration of molecules is increased [27]. The choices of η given in Fig. 4 are simply those that best fit existing experimental data [8].

Figures 5 and 6 show the linewidth and emission intensity at the peak wavelength (620 nm) as a function of pump intensity for different values of transport mean free path l^*. The shapes of these curves are consistent with experimental observations (cf. Fig. 1 in [6]). We see from Fig. 5 that the linewidth is narrowed to about 7 nm at high enough pump
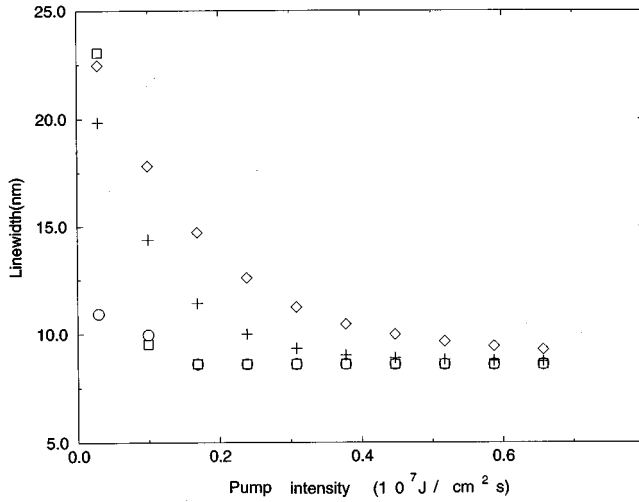
FIG. 5. Linewidth as a function of pump intensity at four different values of the transport mean free path. Transport mean free paths of 1.95×10^{-4}, 1.95×10^{-2}, 1.95×10^{-1}, and 4.88×10^{-1} cm are shown by diamonds, crosses, boxes, and circles, respectively. We set the absorption length $l_a = 2.5 \times 10^{-3}$ cm and the triplet-population parameter $\eta = 0.55$ in the calculations.

intensities and the linewidth vs pump intensity curve is shifted a little bit to the right when we decrease the l^*. The peak emission in Fig. 6 is increased when we decrease the l^* (or, equivalently, as we increase the scatterer density). These results, once again, recapture the experimental observations (cf. Fig. 3 in [2]).

IV. DISCUSSION

The ability of our model to recapture experimental data for certain regimes of scatterer density, dye concentration,
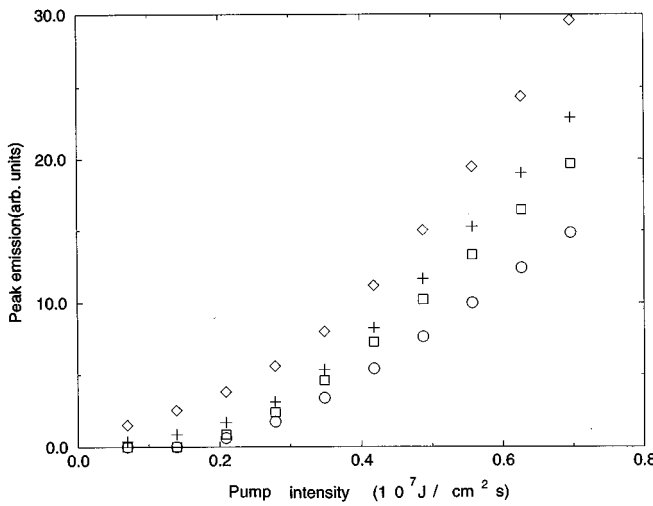

FIG. 6. Emission at the peak wavelength (620 nm) as a function of pump intensity at four different values of the transport mean free path. Transport mean free paths of 1.95×10^{-4}, 1.95×10^{-2}, 1.95×10^{-1}, and 4.88×10^{-1} cm are shown by diamonds, crosses, boxes, and circles, respectively. We set the absorption length $l_a = 2.5 \times 10^{-3}$ cm and the triplet-population parameter $\eta = 0.55$ in the calculations.
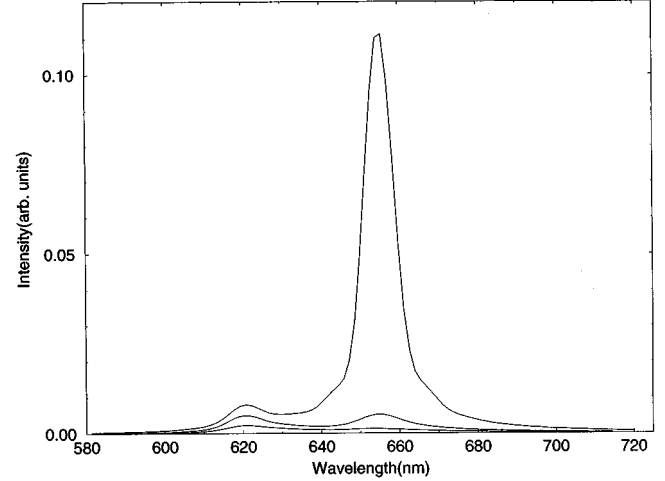

FIG. 7. Example showing that the 650-nm peak occurs prior to the 620-nm peak when the triplet-population parameter is set equal to a higher value. The calculation was done for the system with $l_a = 2.5 \times 10^{-3}$ cm and $l^* = 1.95 \times 10^{-1}$ cm. The pump intensities for these three curves are 0.21×10^7, 0.35×10^7, and 0.42×10^7 J cm^{-2} s^{-1}, respectively. The triplet-population parameter η is set to be 30% higher than that used in Figs. 5 and 6.

and pump beam characteristics suggests that we may use it to predict the behavior of laser paint under different conditions. In order to allow further testing of our theory, we present these predictions. We first note that in our model, the 650-nm peak comes from the triplet states. If this is true, then the energy difference between the lowest levels of the two triplet energy bands, i.e., T_1 and T_2, should be around $\hbar(2\pi c/650 \text{ nm})$. If we increase the pulse duration of the pumping beam or further increase the dye concentration of the random systems (leading to a larger value of η in our model), the 650-nm peak becomes larger than the 620-nm peak (or only the 650-nm peak appears) in our numerical calculations. Figure 7 shows an example of this observation. If we increase the TiO$_2$ particle density such that the transport mean free path is close to the peak wavelength (620 nm), the peak emission increases according to a power law, i.e., $I_{\text{peak}} \sim (l^*/\lambda_0)^{-\alpha}$, where α is a constant that may depend on the dye concentrations and the sample thickness, but not the pumping intensity. This is shown in Figs. 8(a) and 8(b), where we plot our predicted peak emission as a function of the transport mean free path at different pump intensities for different dye concentrations. In these figures, $\alpha = 1.4$–1.5.

From Fig. 8 we also see that there is a peak in the curves around $l^* = 1000\lambda_0$ (which is about an order of magnitude larger than l_z). To the left of this peak around $l^* = 100\lambda_0$ (which is approximately several times l_z, in the figures), the emission at the peak wavelength 620 nm decreases instead of increasing when we lower the transport mean free path. The appearance of this peak around $l^*/\lambda_0 = 1000$ is a geometric effect, which can be explained as follows. In (11), the output intensity is given by an integral over $\widetilde{z}$ of the product of two factors, namely,

$$I_{\text{out}} \propto \int d\widetilde{z} \left\{ \frac{l_z}{l^*} \exp\left(-\frac{\widetilde{z} l_z}{|\hat{k}_f \cdot \hat{\widetilde{z}}| l^*} \right) \right\} \widetilde{I}(\varpi, \widetilde{z}). \quad (19)$$
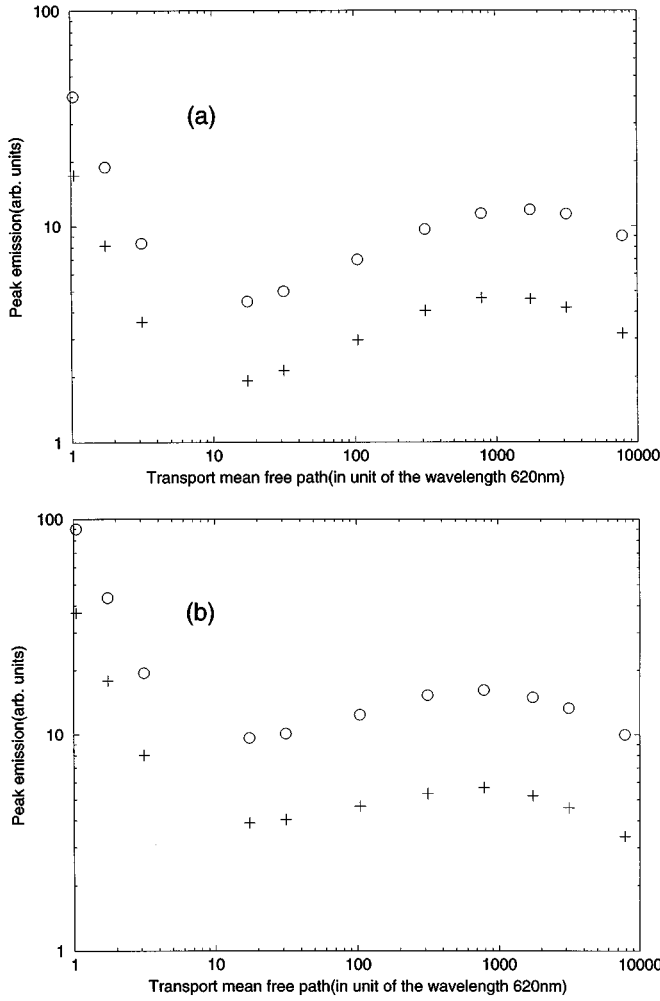
FIG. 8. Emission at the peak wavelength (620 nm) as a function of the transport mean free path at two different pump intensities for two different dye concentrations: (a) low dye concentration with the absorption length $l_a=2.5\times10^{-2}$ cm and the triplet-population parameter $\eta=0.5$ and (b) high dye concentration with $l_a=2.5\times10^{-3}$ cm and $\eta=0.55$. Pump intensities of 0.56×10^7 and 0.35×10^7 J cm^{-2} s^{-1} are shown by circles and crosses, respectively.
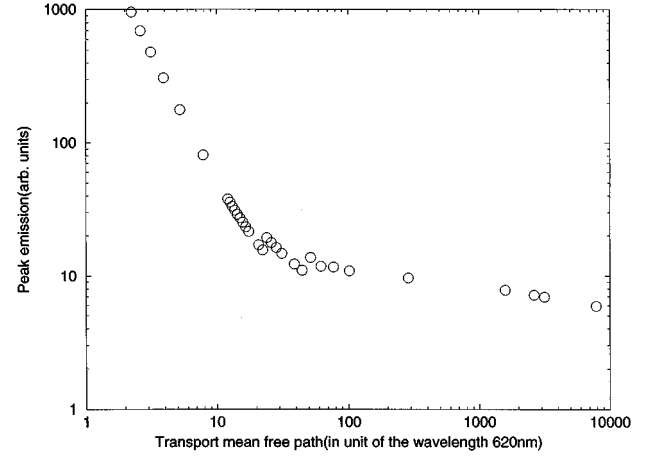

FIG. 9. Emission at the peak wavelength (620 nm) as a function of the transport mean free path in the case when the system is uniformly pumped through the side windows. The dye concentration is set equal to 2.5×10^{-3} M, the pumping intensity is 1.4×10^3 J cm^{-2} s^{-1}, and the sample thickness is 1 cm. Here the triplet population has been set equal to zero for simplicity.

The factor in curly brackets acts as a weight function that describes the probability that the intensity at $\widetilde{z}$ will escape the sample and enter the detector without any further scattering. Due to the decay of the pump beam in the direction [see the factor $e^{-\widetilde{z}}$ in (12)], the $\widetilde{I}(\overline{\omega},\widetilde{z})$ in (19), as a function of z, first increases to a maximum value in a short distance $z\equiv d_p$ (which is approximately several times l_z) and then decays exponentially in the z direction (see Fig. 1). As l^* decreases, the function $\widetilde{I}(\overline{\omega},\widetilde{z})$ grows rapidly because the photon path length in the gain region increase as $(L/l^*)^2$ and this in turn leads to large amplification. However, as l^* decreases, the penetration depth of the weight function decreases as well. When l^* approaches d_p from above, I_{out} exhibits a peak. When l^* falls below d_p, the weight function can no longer access the peak of the stimulated emission intensity $\widetilde{I}(\overline{\omega},\widetilde{z})$ and so the integrated output I_{out}, at the *front window*, decreases at first. As l^* decreases further, the loss of penetration of the weight factor is more than compensated by the overall increase in $\widetilde{I}(\overline{\omega},\widetilde{z})$ and the shift in the peak in $\widetilde{I}$ to small z. If, on the other hand, the output intensity is measured from the *side window* of the sample, then the entire function $\widetilde{I}(\overline{\omega},\widetilde{z})$ is accessible to the detector. In this case I_{out} increases monotonically with decreasing l^*.

Alternatively, if the system is uniformly pumped through the side windows, the factor $e^{-\widetilde{z}}$ in Eq. (12) that describes the decay of the pump beam should be replaced by unity. In this case $d_p=L/2$ and I_{out}, once again, increases monotonically with decreasing l^*. This is shown in Fig. 9, where we plot the peak emission when the pump beam decay factor is absent.

We have also calculated the threshold for the case when the system is uniformly pumped through the side windows. The result is shown in Fig. 11. Here the threshold intensity is determined from a log-log plot of the peak emission vs pump intensity curve, as shown in Fig. 10, where the up arrow indicates the position at which the slope of the curve has a sharp change. This also corresponds to the intensity at which the linewidth collapse is observed. We see from Fig. 11 that the threshold intensity decreases when the transport mean free path decreases.

The power-law increase in amplified emission with decreasing l^* suggests that, in future experiments with stronger scatterers, considerable synergy may be observed between laser activity and photon localization. It was suggested earlier [4] that the macroscopic optical absorption coefficient would be enhanced near a photon mobility edge. This arises from the renormalization of the photon diffusion coefficient to very small values as a result of wave interference corrections to diffusion. At a mobility edge the photon time of flight τ across the sample thickness L scales as $(l^*/c)(L/l^*)^3$ rather than the standard classical diffusion time of flight $\tau\sim(l^*/c)(L/l^*)^2$. This substantial increase in the photon's effective path length and the corresponding increase in light amplification should provide a dramatic signature of the photon localization transition in an active, disordered medium. As mentioned earlier, at the localization transition, the interfering photon diffusion modes are transformed into a continuous spectrum of localized cavity
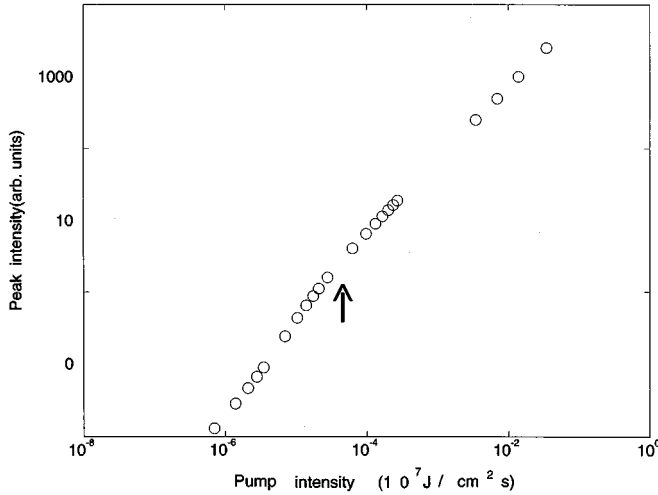
FIG. 10. Emission at the peak wavelength (620 nm) vs the pump intensity on a logarithmic scale. The up-arrow indicates the position of the threshold defined in this paper. The system is uniformly pumped through the side windows and the sample thickness is equal to 1 cm. The dye concentration and the transport mean free path are chosen as 2.5×10^{-3} M and 0.195 cm, respectively, in the calculation. The triplet population has been set equal to zero for simplicity.

modes. These cavity modes have a large (divergent) localization length at the photon mobility edge. Nevertheless, strong feedback effects arising from wave interference and coherent backscattering will be present in this strong scattering limit. These feedback effects are relevant to the development of laser activity. It would be of considerable interest to determine the coherence properties of amplified light emission, starting from the classical diffusion regime ($l^{*}\gg\lambda_0$) for weak scattering and then passing to the photon localization threshold [$l^{*}(2\pi/\lambda_0)\simeq1$] for strong scattering. Future experiments along this lines may prove to be highly rewarding.
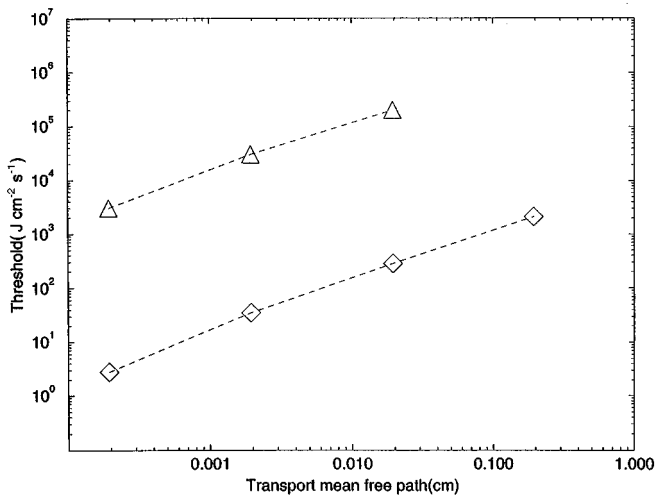

FIG. 11. Variation of the threshold intensity with the transport mean free path in the case when the system is uniformly pumped through the side windows. Diamonds and triangles correspond to sample thicknesses of 1 and 0.1 cm, respectively. The dye concentration is set equal to 2.5×10^{-3} M in the calculations. The triplet population has been set equal to zero for simplicity.

APPENDIX

In the proposed lasing scheme for the R640 dye solution, we assume that the total population in the triplet states is equal to $\eta N_2^{(S)}$ in the pulse duration of the pumping beam, where $N_2^{(S)}$ is the population at the lowest sublevel in S_1 (see Fig. 2). In this appendix we give a justification of this assumption for an ideal case.

We consider the case that

$$(\Gamma_2^{(S)})^{-1}\ll\tau_{\text{pump}}\ll(\kappa_{ST})^{-1}\ll(\kappa_{TS})^{-1}. \tag{A1}$$

where $(\Gamma_2^{(S)})^{-1}$ is the spontaneous-emission lifetime of the lowest level in S_1, τ_{pump} is the pulse duration of the pumping beam, and κ_{ST} (κ_{TS}) is the intersystem crossing rate from the singlet (triplet) to the triplet (singlet) states.

Due to the intersystem crossing process, the total populations in the singlet states and triplets states vary with time and satisfy the rate equations

$$\frac{d}{dt}N_{\text{total}}^{(S)}=-\kappa_{ST}N_2^{(S)}+\kappa_{TS}N_0^{(T)},$$
$$\frac{d}{dt}N_{\text{total}}^{(T)}=\kappa_{ST}N_2^{(S)}-\kappa_{TS}N_0^{(T)}, \tag{A2}$$

where $N_{\text{total}}^{(S)}$ ($N_{\text{total}}^{(T)}$) is the total population in the singlet (triplet) states, $N_2^{(S)}$ is the population in the lowest level of S_1, and $N_0^{(T)}$ is the population in the lowest level of T_1 (see Fig. 2). Because of (A1), the emission processes within the singlet and triplet manifolds are much faster than the intersystem crossing process. In analogy to the adiabatic approximation used in the theory of electronic excitation in a two-atom systems, we can consider $N_{\text{total}}^{(T)}$ (like the distance between the two atoms) as a frozen parameter during the time scale of the emission processes within the singlet and triplet manifolds. Likewise, the total population in the singlet states is fixed at $N-N_{\text{total}}^{(T)}$, where N is the total number of the dye molecules. This results in the separate rate equations for the singlet and triplet manifolds we have written down in Sec. II. On the other hand, when we deal with the intersystem crossing process we can consider the emission processes within the singlet and triplet manifolds to be always in a equilibrium (or steady) state.

Now, according to (A2), the total population in the triplet states at time τ_{pump} is given by

$$N_{\text{total}}^{(T)}=\int_0^{\tau_{\text{pump}}}dt[\kappa_{ST}N_2^{(S)}-\kappa_{TS}N_0^{(T)}]$$
$$\approx[\kappa_{ST}N_2^{(S)}-\kappa_{TS}N_0^{(T)}]\tau_{\text{pump}} \tag{A3}$$

provided that $\tau_{\text{pump}}\ll(\kappa_{ST})^{-1}$. Due to (A1), $N_0^{(T)}<N_{\text{total}}^{(T)}<N_2^{(S)}$ and the second term in (A3) is much smaller than the first term. It follows that

$$N_{\text{total}}^{(T)}\approx\kappa_{ST}\tau_{\text{pump}}N_2^{(S)}, \tag{A4}$$

where $\eta\approx\kappa_{ST}\tau_{\text{pump}}$.

[1] N. M. Lawandy *et al.* (unpublished).

[2] N. M. Lawandy *et al.*, Nature **368**, 436 (1994).

[3] G. Haag *et al.*, IEEE J. Quantum Electron **QE-19**, 1149 (1983); L. G. Nair and K. Dasgupta, *ibid.* **QE-21**, 1782 (1985).

[4] S. John, Phys. Rev. Lett. **53**, 2169 (1984).

[5] S. John, Phys. Today **44** (5), 32 (1991).

[6] R. M. Balachandran and N. M. Lawandy, Opt. Lett. **20**, 1271 (1995).

[7] D. S. Wiersma, M. P. van Albada, and Ad Lagendijk, Nature **373**, 203 (1995); N. M. Lawandy and R. M. Balachandran, *ibid.* **373**, 204 (1995).

[8] W. L. Sha, C.-H. Liu, and R. R. Alfano, Opt. Lett. **19**, 1922 (1994).

[9] D. Zhang *et al.*, Opt. Commun. **118**, 462 (1995).

[10] V. S. Letokhov, Zh. Eksp. Teor. Fiz. **53**, 1442 (1967) [Sov. Phys. JETP **26**, 835 (1968)].

[11] O. Svelto and D. C. Hanna, *Principles of Lasers* (Plenum, New York, 1989); *Dye Lasers*, edited by F. P. Schäfer (Springer, Berlin., 1977).

[12] P. W. Anderson, Philos. Mag. B **52**, 505 (1985).

[13] S. John, in *Confined Electrons and Photons*, Vol. 340 of *NATO Advanced Study Institute, Series B: Physics*, edited by E. Burstein and C. Weisbuch (Plenum, New York, 1995), p. 523.

[14] With some minor changes (see below), our theory can also be applied to the case when we measure the emission from side windows (see D. S. Wiersma, M. P. van Albada, and Ad Lagendijk, Ref. [7]).

[15] D. S. Wiersma, M. P. van Albada, and Ad Lagendijk, Phys. Rev. Lett. **75**, 1739 (1995).

[16] P. Pradhan and N. Kumar, Phys. Rev. B **50**, 9644 (1994).

[17] E. Akkermans, P. E. Wolf, and R. Maynard, Phys. Rev. Lett. **56**, 1471 (1986).

[18] B. Davison and J. B. Sykes, *Neutron Transport Theory* (Oxford University Press, New York, 1957); A. Ishimaru, *Wave Propagation and Scattering in Random Media* (Academic, New York, 1978), Vol. 1.

[19] A. M. Weinberg and E. P. Wigner, *Physical Theory of Neutron Chain Reactors* (University of Chicago, Chicago, 1958).

[20] Th. M. Nieuwenhuizen and J. M. Luck, Phys. Rev. E **48**, 569 (1993).

[21] K. M. Case and P. F. Zweifel, *Linear Transport Theory* (Addison Wesley, Reading, MA, 1967).

[22] F. C. MacKintosh and S. John, Phys. Rev. B **40**, 2383 (1989).

[23] S. John, G. Pang, and Y. Yang, J. Biomed. Opt. **1** (2), 180 (1996).

[24] P. R. Hammond, Appl. Opt. **18**, 536 (1979); T. Efthimiopoulos and B. K. Garside, Can. J. Phys. **59**, 820 (1981).

[25] O. Svelto and D. C. Hanna, *Dye Lasers* (Ref. [11]), p. 160.

[26] *Modern Numerical Methods for Ordinary Differential Equations* edited by G. Hall and J. M. Watt (Clarendon, Oxford, 1976).

[27] A study of the dependence of the intersystem crossing rate and the triplet state lifetime, for rhodamine 6G dye in alcohol, on the dye concentration may be found in J. P. Webb *et al.*, J. Chem. Phys. **53**, 4227 (1970).